Hole-Conductor-Free, Metal-Electrode-Free TiO$_2$/CH$_3$NH$_3$PbI$_3$ Heterojunction Solar Cells Based on a Low-Temperature Carbon Electrode

Huawei Zhou,[†] Yantao Shi,*,[†] Qingshun Dong,[†] Hong Zhang,[†] Yujin Xing,[†] Kai Wang,[†] Yi Du,[†] and Tingli Ma*,[†,‡]

[†]State Key Laboratory of Fine Chemicals, School of Chemistry, Dalian University of Technology, Dalian 116024, China

[‡]Graduate School of Life Science and Systems Engineering, Kyushu Institute of Technology, 2-4 Hibikino, Wakamatsu, Kitakyushu, Fukuoka 808-0196, Japan

S *Supporting Information*

ABSTRACT: Low cost, high efficiency, and stability are straightforward research challenges in the development of organic−inorganic perovskite solar cells. Organolead halide is unstable at high temperatures or in some solvents. The direct preparation of a carbon layer on top becomes difficult. In this study, we successfully prepared full solution-processed low-cost TiO$_2$/CH$_3$NH$_3$PbI$_3$ heterojunction (HJ) solar cells based on a low-temperature carbon electrode. Power conversion efficiency of mesoporous (M-)TiO$_2$/CH$_3$NH$_3$PbI$_3$/C HJ solar cells based on a low-temperature-processed carbon electrode achieved 9%. The devices of M-TiO$_2$/CH$_3$NH$_3$PbI$_3$/C HJ solar cells without encapsulation exhibited advantageous stability (over 2000 h) in air in the dark. The ability to process low-cost carbon electrodes at low temperature on top of the CH$_3$NH$_3$PbI$_3$ layer without destroying its structure reduces the cost and simplifies the fabrication process of perovskite HJ solar cells. This ability also provides higher flexibility to choose and optimize the device, as well as investigate the underlying active layers.

SECTION: Energy Conversion and Storage; Energy and Charge Transport
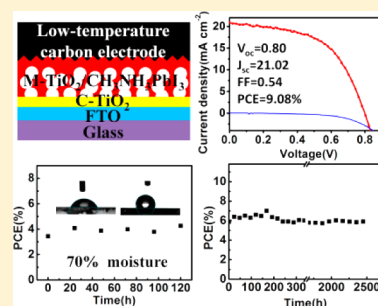
Organolead halide has attracted significant attention as a light harvester for mesoscopic solar cells because of its tunable band gap,[1−3] large absorption coefficient, high charge carrier mobility,[4] and long electron−hole diffusion.[5,6] Methylammonium lead iodide (CH$_3$NH$_3$PbI$_3$) was deposited in a single-step reaction using a mixture of PbI$_2$ and CH$_3$NH$_3$I in a common solvent on mesoporous (M-)TiO$_2$ films, the pores of which were infiltrated with the hole-conductor spiro-MeOTAD. This mesostructured heterojunction (HJ) perovskite solar cell yielded a 9.7% power conversion efficiency (PCE).[7] Through a sequential deposition method to form the perovskite pigment within the porous TiO$_2$, mesostructured HJ perovskites have achieved an approximately 15% PCE.[8] Inert scaffold Al$_2$O$_3$ introduced in mesosuperstructured perovskite solar cells showed that CH$_3$NH$_3$PbI$_{3−x}$Cl$_x$ fulfills the two primary functions of solar cell operation, namely, light absorption and efficient transport of electrons.[10,11] A simple planar HJ solar cell incorporating vapor-deposited perovskite as the absorbing layer can achieve more than 15% PCE.[12] Etgar et al. reported for the first time 5% efficiency based on hole-conductor-free perovskite solar cells, demonstrating that perovskite could function simultaneously as a light harvester and hole conductor.[13] Removing hole transport materials can improve the stability, reduce the cost, and simplify the fabrication process. Under optimized conditions, this performance improved to 10.85% efficiency for depleted hole-conductor-free perovskites.[14−17]

Although this simple perovskite solar cell is a promising photovoltaic device, several disadvantages hinder its practical application. Corrosion problems occur when silver is in contact with the perovskite film, which is likely due to the formation of silver halide.[18] The high cost of the Au electrode also requires a high-vacuum evaporation technique, thereby limiting its future application. Low-cost carbon may be an ideal material to substitute Au as a back contact in perovskite HJ solar cells because its function is similar to that of Au. However, perovskite organic lead iodide is unstable at high temperatures or in some solvents.[19] Thus, the direct preparation of a carbon layer becomes difficult. Recently, Han et al. infiltrated CH$_3$NH$_3$PbI$_3$ into a high-temperature monolithic device of a dye-sensitized solar cell (TiO$_2$ dense layer/TiO$_2$ mesopore layer/ZrO$_2$ space layer/carbon layer).[20−23] However, all of these devices required processing temperatures of up to 400 °C to remove the template in the ZrO$_2$ space layer and carbon layer, which increased the energy consumption and limited their mass production and fabrication on a plastic substrate. Mathews et al. fabricated a carbon nanotube network by chemical vapor deposition method and transferred it onto a CH$_3$NH$_3$PbI$_3$ substrate.[24] However, the preparation of the
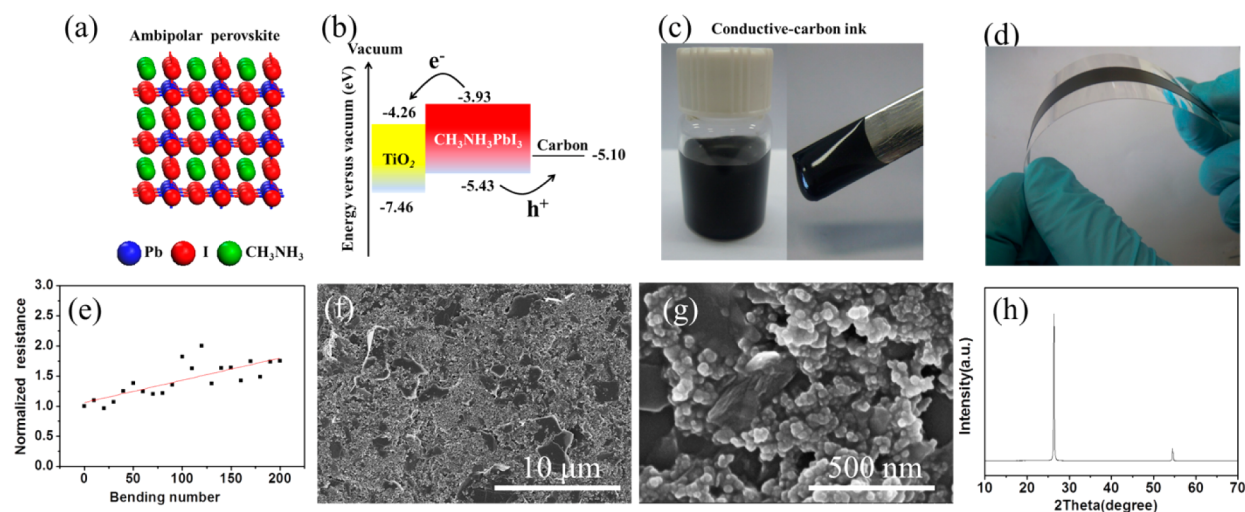
Figure 1. (a) The crystal structure of CH₃NH₃PbI₃; (b) energy-level diagram of TiO₂, CH₃NH₃PbI₃, and carbon; (c) images of conductive carbon ink; (d) conductive carbon film prepared on a plastic substrate at 70 °C; (e) normalized resistance of the carbon film after 200 times of bending the substrate at almost 120°; the linear fit is provided as a guide. (f,g) Top-view SEM of a carbon electrode prepared on a CH₃NH₃PbI₃ layer; (h) XRD of a carbon film prepared by conductive carbon ink at 70 °C on glass.

carbon nanotube network required processing temperatures of up to 1150 °C.

In this study, we successfully prepared TiO₂/CH₃NH₃PbI₃ HJ solar cells based on a low-temperature carbon electrode. M-TiO₂/CH₃NH₃PbI₃/C HJ solar cells based on a low-temperature processing carbon electrode achieved 9.08% PCE. The devices of M-TiO₂/CH₃NH₃PbI₃/C HJ solar cells without encapsulation exhibited advantageous stability (over 2000 h) in air in the dark. The potential to directly process low-cost carbon electrodes at low temperature on top of CH₃NH₃PbI₃ without destroying its structure offers numerous possibilities to choose and optimize the materials and structure of the device.

Figure 1a shows the crystal structure of CH₃NH₃PbI₃. CH₃NH₃PbI₃ is simultaneously a light harvester and a hole conductor because of its ambipolar property. The energy-level diagram of TiO₂, CH₃NH₃PbI₃, and carbon is presented in Figure 1b. The electrons and hole inject efficiently into an n-type semiconductor and carbon electrode, respectively, because of an ambipolar perovskite and energy-level alignment. Given the instability of perovskite organic lead iodide at high temperatures (>150 °C), a low-temperature deposited carbon electrode is necessary. Figure 1c presents photographs of conductive carbon ink prepared by treating the commercial conductive carbon paste. The detailed procedure can be seen the Experiement Methods section. The carbon electrode could be formed at low temperature by the doctor-blade coating method. As we all known, good connectivity and mechanical performance of the carbon film are very important for hole collection and reduce resistance in solar cells. To evaluate the mechanical performance of the carbon layer, we prepared a carbon layer on a flexible polyimide substrate by doctor-blade coating at 70 °C, as shown in Figure 1d. Bending tests indicate that less than a two-fold increase in the resistance of carbon film was observed after being bent 200 times to 120°, as shown in Figure 1e. An adhesion test indicated that no obvious carbon nanoparticles were peeled off from the carbon layer prepared on top of the CH₃NH₃PbI₃ layer, as shown in Figure S1 (Supporting Information). Figure 1f and g shows the top-view scanning electron microscopy (SEM) of the carbon electrode prepared on the CH₃NH₃PbI₃ layer. As shown in the amplified

top-view SEM of the carbon electrode in Figure 1g, the carbon nanoparticle (approximately 18 nm) and flaky graphite (approximately 5 μm) are connected to one another by adhesive resin. This connected nanostructure is a benefit to reducing the resistance of interparticle boundaries, enhacing the mechanical performance and adhesion. These facile fabrication processes at low temperature without high vacuum are promising for future production of all flexible perovskite solar cells. Figure 1h shows the X-ray diffraction (XRD) patterns of the carbon electrode. The narrow peaks at 26 and 54° were obtained from flaky graphite.

Figure 2a shows the designed architectures of the M-TiO₂/CH₃NH₃PbI₃/C HJ solar cell in this study. M-TiO₂ films were prepared by spin-coating a solution of colloidal anatase particles onto a C-TiO₂ blocking layer. CH₃NH₃PbI₃ was prepared according to the two-step sequential deposition method.[9] Carbon electrodes were prepared by doctor-blade coating and

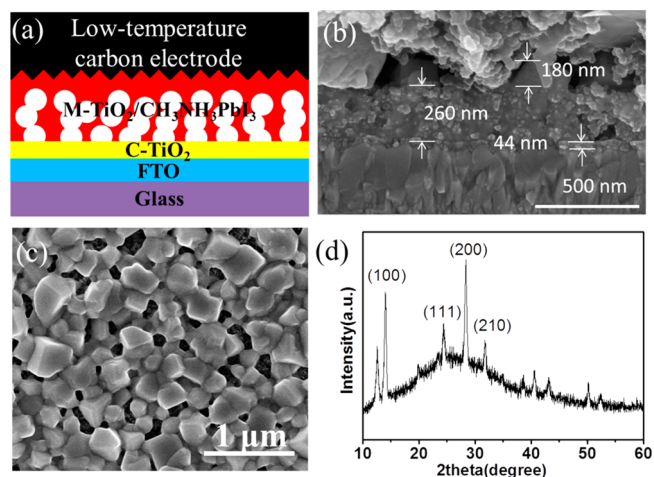**Figure 2.** (a) Schematic designed architectures of M-TiO₂/CH₃NH₃PbI₃/C HJ solar cell; (b) cross-sectional SEM of M-TiO₂/CH₃NH₃PbI₃/C HJ solar cells; (c) top-view SEM of CH₃NH₃PbI₃ on M-TiO₂; (d) XRD spectra of compact (C-)TiO₂/M-TiO₂/CH₃NH₃PbI₃ on glass.
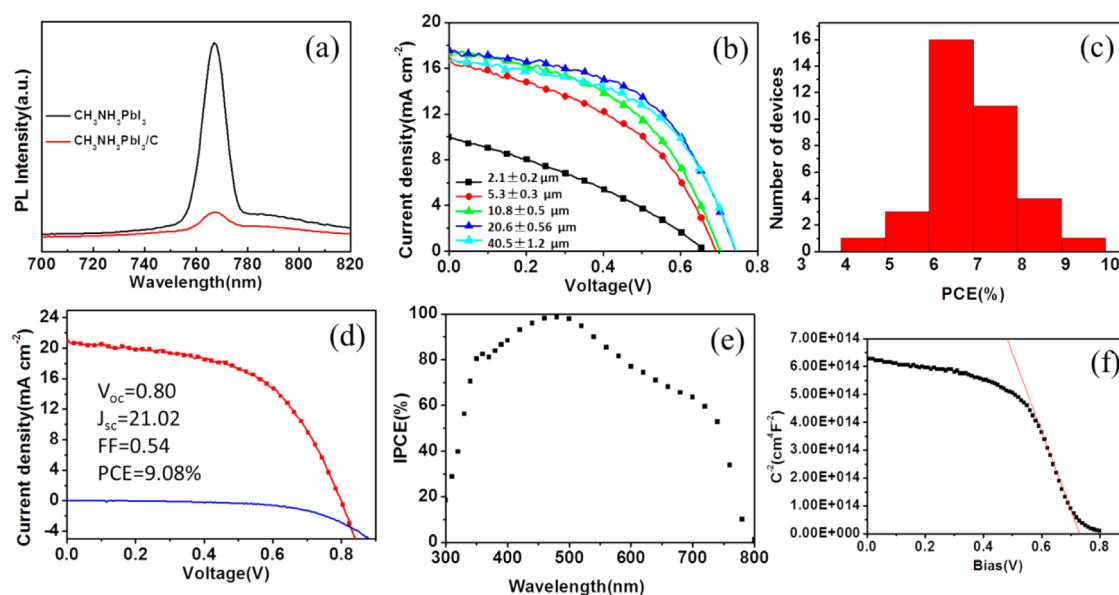
Figure 3. (a) PL of $CH_3NH_3PbI_3$ and $CH_3NH_3PbI_3/C$ on a glass substrate; (b) $J-V$ curves of a M-TiO_2/$CH_3NH_3PbI_3$/C HJ solar cell based on different thicknesses of carbon electrodes; (c) histograms of the PCEs for 36 separate M-TiO_2/$CH_3NH_3PbI_3$/C HJ solar cells; (d) $J-V$ characteristics of the best-performing M-TiO_2/$CH_3NH_3PbI_3$/C HJ solar cell based on a low-temperature carbon electrode and measured at a simulated AM1.5G solar irradiation of 100 mW cm (red line) and in the dark (blue line); (e) IPCE spectrum of the M-TiO_2/$CH_3NH_3PbI_3$/C HJ solar cell; (f) Mott−Schottky plot of the M-TiO_2/$CH_3NH_3PbI_3$/C HJ solar cell.

Table 1. Detailed Photovoltaic Parameters of M-TiO_2/$CH_3NH_3PbI_3$/C HJ Solar Cell Based on Different Thickness of Carbon Electrodes[a]

carbon electrode		M-TiO_2/$CH_3NH_3PbI_3$/C HJ solar cell				
thickness (μm)	square resistanc e(Ω)	V_{oc} (V)	J_{sc} (mA/cm^2)	FF	PCE/%	series resistance (Ω)
2.1 ± 0.2	160 ± 10	0.67 ± 0.02	10.10 ± 0.50	0.33 ± 0.01	2.25 ± 0.18	190 ± 4.3
5.3 ± 0.3	39.3 ± 0.51	0.70 ± 0.02	16.39 ± 1.01	0.43 ± 0.02	5.15 ± 0.37	52.5 ± 2.6
10.8 ± 0.5	21.1 ± 0.42	0.73 ± 0.03	17.19 ± 2.34	0.49 ± 0.04	6.09 ± 0.25	25.2 ± 1.4
20.6 ± 0.56	10.7 ± 0.22	0.75 ± 0.01	17.30 ± 1.07	0.53 ± 0.01	6.90 ± 0.28	19.6 ± 0.88
40.5 ± 1.2	8.2 ± 0.15	0.76 ± 0.02	16.27 ± 0.83	0.53 ± 0.01	6.6 ± 0.42	18.5 ± 0.50

[a]The error for photovoltaic parameters in Table 1 is calculated by four separate cells for each film thickness.

dried at 70 °C for 40 min. Further experimental details are provided in the Experiment Methods section. Figure 2b displays a cross-sectional SEM image of M-TiO_2/$CH_3NH_3PbI_3$/C HJ solar cells. The thickness of C-TiO_2 is approximately 44 nm. The M-TiO_2 film is approximately 260 nm thick, and the $CH_3NH_3PbI_3$ perovskite is infiltrated into the pore of the TiO_2 film. In addition, a large crystal of $CH_3NH_3PbI_3$ can be observed on top of the TiO_2 film with a wide range of sizes between 180 and 310 nm. The large crystal is also seen clearly from the top-view SEM of $CH_3NH_3PbI_3$ on M-TiO_2 (Figure 2c). The XRD pattern of the $CH_3NH_3PbI_3$ on the M-TiO_2 film can be seen in Figure 2d. Strong diffraction peaks at 14.05, 24.35, 28.34, and 31.88° correspond to the (100), (111), (200), and (210) lattice planes of $CH_3NH_3PbI_3$.[8] The diffraction peaks at 12.6° can be attributed to the PbI_2 impurity.[9]

To determine whether the carbon electrode formed by conductive carbon ink can function as a hole acceptor within the M-TiO_2/$CH_3NH_3PbI_3$/C HJ solar cell, we estimate the photoluminescence (PL) quenching of the perovskite emission. Figure 3a shows that the PL of $CH_3NH_3PbI_3$ on bare glass has strong luminescence at ~767 nm. Although the sample of glass/$CH_3NH_3PbI_3$/C has stronger absorption from 600 to 800 nm than that of glass/$CH_3NH_3PbI_3$ (as shown in Figure S2,

Supporting Information), a carbon electrode prepared by low temperature quenches the perovskite steady-state PL. According to the band edge positions of TiO_2, $CH_3NH_3PbI_3$, and C, the energy-level diagram of the M-TiO_2/$CH_3NH_3PbI_3$/C HJ solar cell is shown in Figure 2b. Thus, the carbon electrode has a dual role in the M-TiO_2/$CH_3NH_3PbI_3$/C HJ solar cell system. First, it is used as a hole acceptor. Second, it works as a conductive electrode to transport holes to the external circuit. Thus, suitable band edge position and high electrical conductivity are desirable in the M-TiO_2/$CH_3NH_3PbI_3$/C HJ solar cell system. The thickness of carbon film influences the electrical conductivity. Figure 3b shows the current density (J)−voltage (V) characteristics of M-TiO_2/$CH_3NH_3PbI_3$/C HJ solar cells based on different thicknesses of carbon electrodes. The detailed photovoltaic parameters are shown in Table 1. When the thickness is 2.1 ± 0.2 μm, the devices have rather poor photovoltaic performance, which can be attributed to high square resistance (160 ± 10 Ω) of a carbon electrode and high series resistance of the device (190 ± 4.3 Ω). The square resistance and series resistance were reduced as the thickness of the carbon electrode increased. The fill factor (FF) is closely connected to series resistance in solid solar cells. A significant increase in the fill factor (from 0.33 ± 0.01 to 0.53 ± 0.01) of the photovoltaic devices resulted in an increase in the PCE
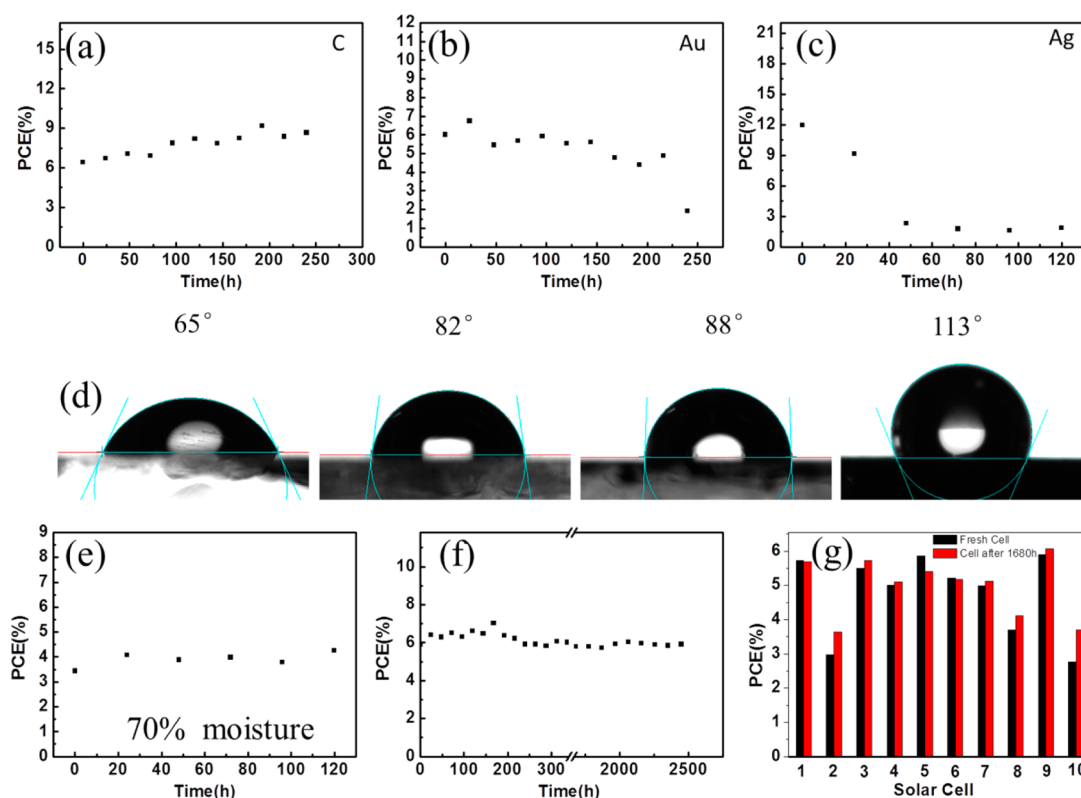
Figure 4. (a) Stability of M-TiO$_2$/CH$_3$NH$_3$PbI$_3$/C HJ solar cells without encapsulation in air in the dark; (b) stability of M-TiO$_2$/CH$_3$NH$_3$PbI$_3$/spiro-OMeTAD/Au without encapsulation in air in the dark; (c) stability of M-TiO$_2$/CH$_3$NH$_3$PbI$_3$/Spiro-OMeTAD/Ag without encapsulation in air in the dark; (d) contact angles for H$_2$O on carbon, Au, and Ag surfaces in a full cell: the first one (M-TiO$_2$/CH$_3$NH$_3$PbI$_3$/Au cell); the second one (M-TiO$_2$/CH$_3$NH$_3$PbI$_3$/spiro-OMeTAD/Au cell); the third one (M-TiO$_2$/CH$_3$NH$_3$PbI$_3$/spiro-OMeTAD/Ag cell); the fourth one (M-TiO$_2$/CH$_3$NH$_3$PbI$_3$/C cell). (e) Stability of M-TiO$_2$/CH$_3$NH$_3$PbI$_3$/C HJ solar cells without encapsulation in 70% moisture in the dark; (f) long stability of M-TiO$_2$/CH$_3$NH$_3$PbI$_3$/C HJ solar cells without encapsulation in air in the dark; (g) long stability of 10 separate M-TiO$_2$/CH$_3$NH$_3$PbI$_3$/C HJ solar cells without encapsulation in air in the dark (black: fresh cell; red: fresh cell after 1680 h).

(from 2.25 ± 0.18 to 6.90 ± 0.28%). The photovoltaic devices with approximately 20 μm thickness of carbon electrodes have the best performance. To confirm the reproducibility of the results, 36 separate devices were fabricated and tested using the optimized carbon electrode thickness (approximately 20 μm). Histograms of PCEs are shown in Figure 3c. More than 88% of the cells show a PCE above 6%. More than 10% show a PCE above 8%. Figure 3d shows the J–V curves for the best-performing device. The values for the short-circuit photocurrent (J_{sc}), open-circuit voltage (V_{oc}), FF, and PCE are 21.02 mA cm^{-2}, 800 mV, 0.54, and 9.08%, respectively. This performance of M-TiO$_2$/CH$_3$NH$_3$PbI$_3$/C HJ solar cells based on a low-temperature-processed carbon electrode can be comparable to the cell based on a high-temperature carbon electrode.[20−24] The incident-photon-to-current conversion efficiency (IPCE) for the perovskite cell is presented in Figure 3e. The value of the IPCE starts at 800 nm, corresponding to the band gap of CH$_3$NH$_3$PbI$_3$, and reaches 99% at almost 480 nm. To estimate the built-in potential, we performed Mott–Schottky analysis on the M-TiO$_2$/CH$_3$NH$_3$PbI$_3$/C HJ solar cell. The results are shown in Figure 3f. According to junction capacitance (eq 1), the built-in potential can be extrapolated using the intercept of the linear regime with the x-axis of the Mott–Schottky plot, which is equal to 0.73 V, consistent with the V_{oc} of the photovoltaic device. The presence of a built-in field can efficiently force the separation of photogenerated carriers and suppress the back reaction of electrons from the M-TiO$_2$ film to the CH$_3$NH$_3$PbI$_3$ layer. Future work will

concentrate on the relationship between the thickness of the depletion region and the performance of the photovoltaic devices.

$$\frac{1}{C^2} = \frac{2}{\varepsilon \varepsilon_0 q A^2 N}(V_{bi} - V) \tag{1}$$

where C is the measured capacitance, A is the active area, V is the applied bias, ε is the static permittivity, ε_0 is the permittivity of free space, q is the elementary charge, and N is the dopping density of the donor.

Finally, the stability of the M-TiO$_2$/CH$_3$NH$_3$PbI$_3$/C HJ solar cell without encapsulation was tested in air in the dark, as shown in Figure 4a. The regular perovskite solar cells with HTM (spiro-OMeTAD) and a metal electrode (Au and Ag) as a control study were prepared and tested under the same condition, as shown in Figure 4b and c. Compared with the regular perovskite solar cell with spiro-OMeTAD and a metal electrode, the M-TiO$_2$/CH$_3$NH$_3$PbI$_3$/C HJ solar cell exhibited better stability. The changes in V_{oc}, J_{sc}, and FF for three kinds of solar cell are shown in Figure S3 (Supporting Information). The perovskite solar-cell-based Ag electrode exhibited poor stability because Ag would be corroded by CH$_3$NH$_3$PbI$_3$ penetrating from the spiro-OMeTAD layer. In addition, HTM and its volatile additives may be another reason for the instability for regular perovskite solar cells with spiro-OMeTAD and a metal electrode. The contact angles for H$_2$O on carbon, Au, and Ag surfaces in full cells could be seen in Figure 4d. The

contact angle on Au and Ag in the full cell is less than 90°, indicating that their hydrophilic surface could be partially wetted by H_2O. The contact angle on a carbon electrode in a full cell is 113°, implying that its hydrophobic surface is nonwetted. This hydrophobic surface may be beneficial to the stability of the cells without encapsulation when they are exposed to moisture. The $M-TiO_2/CH_3NH_3PbI_3/C$ HJ solar cell also had good stability in 70% moisture, as shown in Figure 4e. The changes in V_{oc}, J_{sc}, and FF in 70% moisture are shown in Figure S4 (Supporting Information). Figure 4f shows that the PCE value remained at 5.91% after 2446 h for the initial 5.89% efficiency of the $M-TiO_2/CH_3NH_3PbI_3/C$ HJ solar cells without encapsulation in air in the dark. To confirm the reproducibility of the results, 10 separate devices were tested for stability in air, as shown in Figure 4g. After 1680 h, all solar cells can maintain their initial PCEs or 90% of their initial PCEs. The changes in V_{oc}, J_{sc}, and FF for 10 separate devices are displayed in Figure S5 (Supporting Information). Compared to HTM-free cells with a high-vacuum-evaporated Au electrode, this low-cost and stable HTM-free cell with a low-temperature-processed carbon electrode is a very promising photovoltaic devices.

In summary, we have successfully developed a route to create a low-temperature-processed carbon electrode in perovskite HJ solar cells. Low-temperature conductive carbon ink can be directly coated on top of the $CH_3NH_3PbI_3$ layer without destroying it. The $M-TiO_2/CH_3NH_3PbI_3/C$ HJ solar cells based on a low-temperature-processed carbon electrode achieved a 9.08% PCE. The devices of $M-TiO_2/CH_3NH_3PbI_3/C$ HJ solar cells without encapsulation exhibited advantageous stability (over 2000 h) in air in the dark. This study reduces the cost and simplifies the fabrication process of perovskite HJ solar cells, as well as offering numerous possibilities to choose and optimize the materials and structure of the device.

EXPERIMENTAL METHODS

Preparation of Low-Temperature Conductive Carbon Ink: First, low-cost commercial conductive carbon paste was dried at 120 °C for 12 h to remove the solvent, which can destroy the structure of perovskite. Subsequently, the dried conductive carbon sample (5 g) and zirconium dioxide pearl (4 g) were dispersed in chlorobenzene (15 mL) and milled for 2 h in an electromill (QM-QX0.4, Instrument Factory of Nanjing University).

Device Fabrication of $M-TiO_2/CH_3NH_3PbI_3/C$ HJ Solar Cells: Patterned FTO-coated glass substrates were coated with a TiO_2 compact layer by spin-coating the TiO_2 organic sol at 3,000 rpm for 30 s, followed by drying at 450 °C for 30 min. The $M-TiO_2$ layer was coated with a commercial TiO_2 paste (Dyesol 18NRT, Dyesol) diluted in ethanol (1:3.5, weight ratio) by spin coating at 5000 rpm for 30 s, followed by gradual heating to 500 °C, baked at this temperature for 30 min. $CH_3NH_3PbI_3$ was prepared according to a two-step sequential deposition method.[9] Finally, the carbon electrodes were prepared by doctor-blade coating conductive carbon ink on a $CH_3NH_3PbI_3$ layer using different layers of adhesive tapes as pattern and spaces, followed by drying at 70 °C for 40 min.

Measurement and Characterization. The square resistance and film thickness of carbon electrodes were measured using a four-point probe measurement system (RST-9, China) and step profiler (Surfcom 130A, Japan), respectively. XRD patterns were obtained using a PANalyticalX'Pert diffractometer (Cu Kα

radiation at λ = 1.54 Å) sampling at 10°/min, 40 kV, and 100 mA. Nanostructures of our samples were characterized and analyzed by scanning electron microscopy (SEM, Nova Nano SEM 450). Photoluminescence (PL) measurements were taken using an excitation wavelength of 508 nm. The sample was held at a 45° angle with the glass side facing the excitation source and detector. The photocurrent–voltage performance of the DSCs was measured by a Keithley digital source meter (Keithley 2601, U.S.A.) equipped with a solar simulator (PEC-L15, Peccell, Yokohama, Japan). Series resistance and the Mott–Schottky plot of the solar cell was measured in electrochemical impendence spectroscopy (ZenniumZahner, Germany). The active area of the solar cells was defined with a metal aperture mask of about 0.06 cm^2.

ASSOCIATED CONTENT

$\circledS$ Supporting Information

Adhesion test for the carbon electrode. UV–vis absorption spectrum of $CH_3NH_3PbI_3$ and $CH_3NH_3PbI_3/C$ on a glass substrate. The stability of V_{oc}, J_{sc}, and FF for three kinds of solar cells without encapsulation in air in the dark. The stability of V_{oc}, J_{sc}, and FF for a $M-TiO_2/CH_3NH_3PbI_3/C$ HJ solar cell without encapsulation in 70% moisture. The stability of V_{oc}, J_{sc}, and FF for 10 $M-TiO_2/CH_3NH_3PbI_3/C$ HJ solar cells without encapsulation in air in the dark. This material is available free of charge via the Internet at http://pubs.acs.org.

AUTHOR INFORMATION

Corresponding Authors
*E-mail: tinglima@dlut.edu.cn (T.M.).
*E-mail: shiyantao@dlut.edu.cn (Y.S.).

Notes
The authors declare no competing financial interest.

REFERENCES

(1) Eperon, G. E.; Stranks, S. D.; Menelaou, C.; Johnston, M. B.; Herz, L. M.; Snaith, H. J. Formamidinium lead trihalide: a broadly tunable perovskite for efficient planar heterojunction solar cells. *Energy Environ. Sci.* **2014**, 7, 982−988.

(2) Noh, J. H.; Im, S. H.; Heo, J. H.; Mandal, T. N.; Seok, S. I. Chemical management for colorful, efficient, and stable inorganic−organic hybrid nanostructured solar cells. *Nano Lett.* **2013**, 13, 1764−1769.

(3) Mosconi, E.; Amat, A.; Nazeeruddin, M. K.; Graetzel, M.; De Angelis, F. First-principles modeling of mixed halide organometal perovskites for photovoltaic applications. *J. Phys. Chem. C* **2013**, 117, 13902−13913.

(4) Stoumpos, C. C.; Malliakas, C. D.; Kanatzidis, M. G. Semiconducting tin and lead iodide perovskites with organic cations: phase transitions, high mobilities, and near-infrared photoluminescent properties. *Inorg. Chem.* **2013**, 52, 9019−9038.

(5) Stranks, S. D.; Eperon, G. E.; Grancini, G.; Menelaou, C.; Alcocer, M. J. P.; Leijtens, T.; Herz, L. M.; Petrozza, A.; Snaith, H. J. Electron−hole diffusion lengths exceeding 1 micrometer in an organometal trihalide perovskite absorber. *Science* **2013**, 342, 341−344.

(6) Xing, G.; Mathews, N.; Sun, S.; Lim, S. S.; Lam, Y. M.; Graetzel, M.; Mhaisalkar, S.; Sum, T. C. Long-range balanced electron- and

hole-transport lengths in organic−inorganic CH$_3$NH$_3$PbI$_3$. *Science* **2013**, *342*, 344−347.

(7) Kim, H.-S.; Lee, C.-R.; Im, J.-H.; Lee, K.-B.; Moehl, T.; Marchioro, A.; Moon, S.-J.; Humphry-Baker, R.; Yum, J.-H.; Moser, J. E.; et al. Lead iodide perovskite sensitized all-solid-state submicron thin film mesoscopic solar cell with efficiency exceeding 9%. *Sci.Rep.* **2012**, *2*, 519.

(8) Baikie, T.; Fang, Y.; Kadro, J. M.; Schreyer, M.; Wei, F.; Mhaisalkar, S. G.; Graetzel, M.; White, T. J. Synthesis and crystal chemistry of the hybrid perovskite (CH$_3$NH$_3$)PbI$_3$ for solid-state sensitised solar cell applications. *J. Mater. Chem. A* **2013**, *1*, 5628−5641.

(9) Burschka, J.; Pellet, N.; Moon, S.-J.; Humphry-Baker, R.; Gao, P.; Nazeeruddin, M. K.; Graetzel, M. Sequential deposition as a route to high-performance perovskite-sensitized solar cells. *Nature* **2013**, *499*, 316−320.

(10) Lee, M. M.; Teuscher, J.; Miyasaka, T.; Murakami, T. N.; Snaith, H. J. Efficient hybrid solar cells based on meso-superstructured organometal halide perovskites. *Science* **2012**, *338*, 643−647.

(11) Ball, J. M.; Lee, M. M.; Hey, A.; Snaith, H. J. Low-temperature processed meso-superstructured to thin-film perovskite solar cells. *Energy Environ. Sci.* **2013**, *6*, 1739−1743.

(12) Mingzhen, L.; Johnston, M. B.; Snaith, H. J. Efficient planar heterojunction perovskite solar cells by vapour deposition. *Nature* **2013**, *501*, 395−398.

(13) Etgar, L.; Gao, P.; Xue, Z.; Peng, Q.; Chandiran, A. K.; Liu, B.; Nazeeruddin, M. K.; Graetzel, M. Mesoscopic CH$_3$NH$_3$PbI$_3$/TiO$_2$ heterojunction solar cells. *J. Am. Chem. Soc.* **2012**, *134*, 17396−17399.

(14) Abu Laban, W.; Etgar, L. Depleted hole conductor-free lead halide iodide heterojunction solar cells. *Energy Environ. Sci.* **2013**, *6*, 3249−3253.

(15) Jiangjian, S.; Juan, D.; Songtao, L.; Yuzhuan, X.; Lifeng, Z.; Junyan, X.; Xin, X.; Huijue, W.; Dongmei, L.; Yanhong, L.; et al. Hole-conductor-free perovskite organic lead iodide heterojunction thin-film solar cells: high efficiency and junction property. *Appl. Phys. Lett.* **2014**, *104*, 063901/1−063901/4.

(16) Xu, Y.; Shi, J.; Lv, S.; Zhu, L.; Dong, J.; Wu, H.; Xiao, Y.; Luo, Y.; Wang, S.; Li, D.; et al. Simple way to engineer metal−semiconductor interface for enhanced performance of perovskite organic lead iodide solar cells. *ACS Appl. Mater. Interfaces* **2014**, *6*, 5651−5656.

(17) Sigalit, A.; Shany, G.; Bat, E. C.; Lioz, E. Depletion region effect of highly efficient hole conductor free CH$_3$NH$_3$PbI$_3$ perovskite solar cells. *Phys. Chem. Chem. Phys.* **2014**, *16*, 10512−10518.

(18) Leijtens, T.; Eperon, G. E.; Pathak, S.; Abate, A.; Lee, M. M.; Snaith, H. J. Overcoming ultraviolet light instability of sensitized TiO$_2$ with meso-superstructured organometal tri-halide perovskite solar cells. *Nat. Commun.* **2013**, *4*, 2885.

(19) Amalie, D.; Nicolas, T.; Thomas, M.; Peng, G.; Mohammad, K. N.; Michael, G. Effect of annealing temperature on film morphology of organic−inorganic hybrid pervoskite solid-state solar cells. *Adv. Funct. Mater.* **2014**, *24*, 3250−3258.

(20) Ku, Z.; Rong, Y.; Xu, M.; Liu, T.; Han, H. Full printable processed mesoscopic CH$_3$NH$_3$PbI$_3$/TiO$_2$ heterojunction solar cells with carbon counter electrode. *Sci.Rep.* **2013**, *3*, 3132.

(21) Mei, A.; Li, X.; Liu, L.; Ku, Z.; Liu, T.; Rong, Y.; Xu, M.; Hu, M.; Chen, J.; Yang, Y.; et al. A hole-conductor-free, fully printable mesoscopic p erovskite solar cell with high stability. *Science* **2014**, *345*, 295−298.

(22) Xu, M.; Rong, Y.; Ku, Z.; Mei, A.; Liu, T.; Zhang, L.; Li, X.; Han, H. Highly ordered mesoporous carbon for mesoscopic CH$_3$NH$_3$PbI$_3$/TiO$_2$ heterojunction solar cell. *J. Mater. Chem. A* **2014**, *2*, 8607−8611.

(23) Rong, Y.; Ku, Z.; Mei, A.; Liu, T.; Xu, M.; Ko, S.; Li, X.; Han, H. Hole-conductor-free mesoscopic TiO$_2$/CH$_3$NH$_3$PbI$_3$ heterojunction solar cells based on anatase nanosheets and carbon counter electrodes. *J. Phys. Chem. Lett.* **2014**, *5*, 2160−2164.

(24) Li, Z.; Kulkarni, S. A.; Boix, P. P.; Shi, E.; Cao, A.; Fu, K.; Batabyal, S. K.; Zhang, J.; Xiong, Q.; Wong, L. H.; et al. Laminated carbon nanotube networks for metal electrode-free efficient perovskite solar cells. *ACS Nano* **2014**, *8*, 6797−804.

3246

dx.doi.org/10.1021/jz5017069 | *J. Phys. Chem. Lett.* 2014, 5, 3241−3246